Three-dimensional composite metallodielectric nanostructure for enhanced surface plasmon resonance sensing

Haiping Matthew Chen,[a] Lin Pang, Aditya Kher, and Yeshaiahu Fainman
Department of Electrical of Computer Engineering, University of California, San Diego 9500 Gilman Drive, La Jolla, California 92093, USA

(Received 24 November 2008; accepted 28 January 2009; published online 19 February 2009)

The authors simulated, fabricated, and characterized a mushroomlike composite metallodielectric nanostructure that shows improved characteristics for surface plasmon resonance sensing applications with an enhancement in the normal electric field compared to the conventional nanohole structure. A fabrication method is introduced to give controllable linewidth by an oblique metal deposition process. A sensor built with the composite nanostructure was then used to determine the hydrophilicity of its surface by monitoring the resonant wavelength shift and computing the corresponding adsorption thickness. © *2009 American Institute of Physics*.
[DOI: 10.1063/1.3083551]

Since the discovery of extraordinary transmission through subwavelength nanohole arrays,[1] researchers have been exploring its applications in surface plasmon resonance (SPR) sensing as an alternative to the prism-based Kretschmann–Raether configuration[2] and the diffraction grating approach[3–5] with special emphasis on high-throughput.[6–10] Recently, both the sensitivity[7,10,11] and the minimum resolution[12] in two-dimensional (2D) nanohole array SPR sensors have improved significantly.

To further increase sensitivity, researchers have also investigated coupling between localized surface plasmon resonances (LSPRs) and propagating surface plasmon polaritons (SPPs) of double-hole arrays,[11] coaxial metallic arrays,[13] and nanoholes with embedded nanoparticles.[14] In this paper, we present a three-dimensional (3D) composite mushroomlike metallodielectric nanostructure as an alternative approach for coupling these two types of plasmonic phenomena and exploit them for a wide range of practical applications.

The proposed geometry is a layer of structured gold film on top of a perforated substrate, as shown in Fig. 1(a). The size of the voids between the gold can be controlled independently of the underlying cylindrical perforations. When SPPs reflect between gold barriers, they interfere with each other and form localized standing waves.[15] Field localization also occurs near sharp apexes and the coupling between these two mechanisms is used to enhance the normal electric field. The LSPRs exist in the voids, while the SPPs exist on the gold surface. From the SPP dispersion relation for a 2D nanohole structure with a periodicity of 1.2 μm and a laser center wavelength of 1.55 μm, the required plane-wave incidence angle to excite the $(-1, 0)$ air-metal (AM) mode occurs at 17.3°. Considering an incident beam illuminating the array from air at an angle of 17.3°, rigorous coupled wave analysis (RCWA) was used to simulate the transmission in Fig. 1(b) for a 2D nanohole array with a periodicity of 1.2 μm, a gap size of 200 nm, and a gold film thickness of 100 nm.[16] It can be clearly seen that the $(-1, 0)$ AM mode can be excited around 1.55 μm, matching the calculation from the dispersion relation. Figure 1(b) also reveals the excitation of substrate-metal modes with a substrate index of 1.5. The near-field distribution of the electric fields at the SPP resonance was then simulated using the finite element method (FEM). Figure 1(c) shows the near-field distribution for a conventional nanohole structure in a gold film, which has a maximum value of 87 kV/m. On the other hand, an enhanced field distribution for the composite mushroomlike metallodielectric nanostructure is shown in Fig. 1(d) where the maximum value reaches 125 kV/m. The input port power is 1 W in both cases. The field enhancement is not due to the narrower gap, but rather due to couplings between the edges of the mushroomlike shape as well as localized and propagating plasmons. Furthermore, a 25-nm-thick subdomain integration of the normal electric field immediately above the gold material reveals an enhancement factor of 1.4 for the mushroomlike composite nanostructure compared to the 2D nanohole structure.

To fabricate these 3D composite nanostructures over an area of more than 1 cm^2, the holographic lithography based

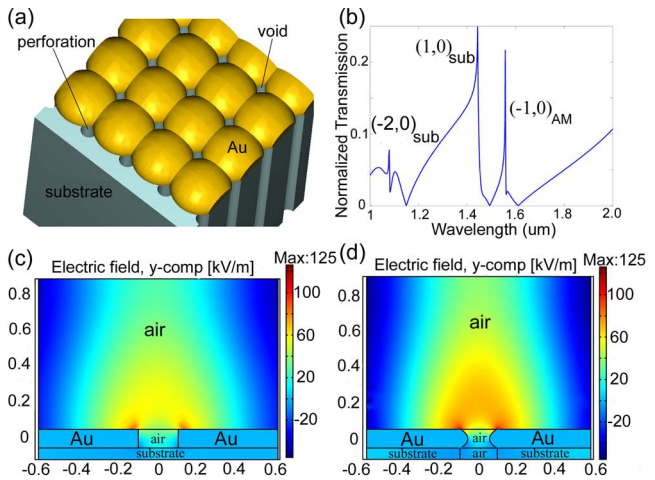

FIG. 1. (Color online) (a) Schematic of the proposed structure utilizing coupling between LSPRs in the voids and SPPs on the gold surface. (b) Far-field RCWA simulation of nanohole array excited at 17.3° with a periodicity of 1.20 μm and a gap size of 200 nm using a gold thickness of 100 nm. (c) Near-field FEM simulation of the conventional nanohole. (d) Composite mushroomlike nanostructure showing an enhancement in the normal electric field at 1.556 μm. Dimensions are in microns and the incident wave is at an angle of 17.3°.

[a]Electronic mail: hpchen@ucsd.edu.

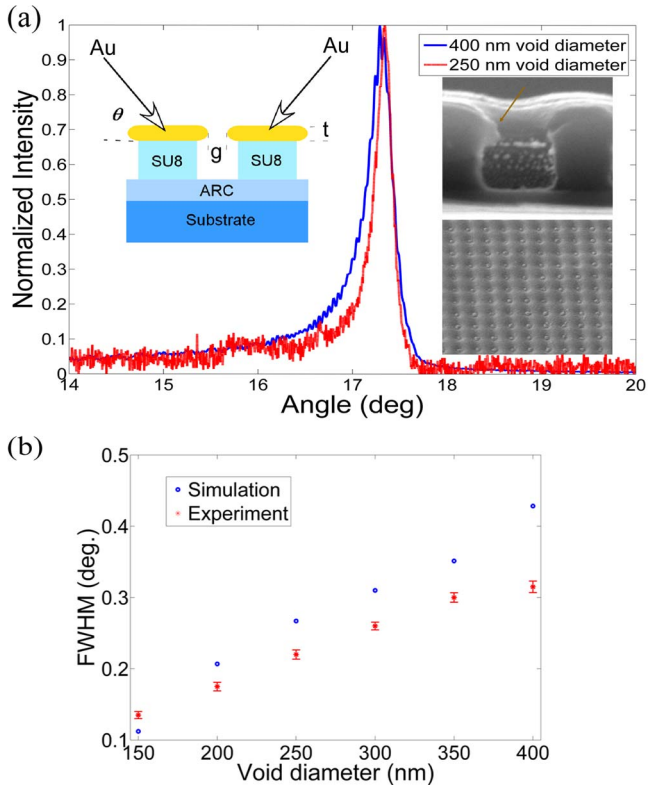

FIG. 2. (Color online) (a) Transmission spectra at a wavelength of 1550 nm with void diameters of 250 and 400 nm with corresponding FWHMs of 0.220° and 0.315°, respectively. The upper left inset illustrates a schematic of how the void size can be controlled by sputtering gold at an oblique angle with the sample on a rotating stage, while the upper right inset shows a cross section of the mushroomlike structure, and the lower right inset reveals that the void had been sealed because the deposition time was too long. (b) A comparison of the angular FWHM vs the void diameter for both simulation and experimental data.

on two-beam interferometry was used. However, with traditional fabrication methods that require a dry etching step, the nanohole size cannot be reduced after the initial exposure; moreover, the mushroomlike shape in the metal film cannot be achieved to yield the higher localized electric fields. Here, we present a paradigm shift, introducing a straightforward fabrication method in which the void size can be controlled and changed even after holographic exposure. As shown in Fig. 2(a), this technique offers simplicity in fabrication and controllable linewidth by varying the void size. It also offers the ability to reconfigure the nanostructure array by stripping away the gold layer and sputtering another film with a different thickness. The fabrication consists of the formation of the nanohole array in polymer and an oblique metal deposition step. The nanohole array is formed in a thick photoresist by using holographic lithography. The deposition is achieved by sputtering a controlled layer of gold from an oblique angle as the substrate is rotated on the deposition stage as shown in the upper inset of Fig. 2(a). The thickness of this layer is given by

$$t = RT \sin \theta, \tag{1}$$

where R, T, and θ are the deposition rate, time, and the incidence angle of ion beam, respectively. The void size, which is the gap shown in the inset of Fig. 2, is determined by

$$g = d - 2RT \cos(\theta) f, \tag{2}$$

where d is the periodicity in the resist and f is a filling factor, empirically calculated to be between 1.1 and 1.3. As the thickness increases, the void size decreases; thus, the size can be precisely controlled by merely adjusting the sputtering time. Since the void size determines the scattering rate (and hence, the lifetime) of the SPP mode, decreasing the size gives a narrower transmission linewidth.[17,18] The full width at half maximum (FWHM) of the resonant linewidth Γ directly dictates the SPR sensor's minimum resolution and resolving power with a figure of merit defined by $\chi = S/\Gamma$, where S is the sensitivity defined as the derivative of the monitored resonant parameter with respect to the refractive index unit. Hence, a narrower linewidth yields a higher figure of merit.

The transmission spectrum was characterized using the setup described in Ref. 7. A comparison of the measured spectra is shown in Fig. 2(a) for void diameters of 400 and 250 nm with corresponding FWHM linewidths of 0.315° and 0.220°, respectively. These two void sizes were obtained from the same sample by stripping the original gold layer and then depositing another layer of a different thickness onto the same SU-8 photoresist array. The upper right inset is a cross-section of the array, depicting the mushroomlike shape of the gold that was deposited as it protrudes out over the resist pillars as pointed by the arrow. The lower right inset reveals that the voids have been sealed due to overdeposition. The strong correlation between the linewidth and the void size verifies that the linewidth can, indeed, be controlled by varying the void size via the gold film thickness with this oblique sputtering technique, as shown in Fig. 2(b). The measurements correspond reasonably well to RCWA simulations with a small discrepancy due to the effects of directly transmitted background, which were included in the simulation but suppressed in the experiment by a polarizer-analyzer arrangement.[7] For void diameters of 150, 200, 250, 300, 350, and 400 nm, the corresponding FWHMs are 0.135°, 0.175°, 0.220°, 0.260°, 0.300°, and 0.315°, respectively.

As an application, the fabricated composite nanostructure array was used to determine the surface hydrophilicity by measuring the resonant wavelength shift in the laser beam transmitted through the 3D nanostructure array, which was bonded to a polydimethylsiloxane (PDMS) chamber. Only the AM mode was monitored because the required wavelength to excite the liquid-metal mode is outside of the laser's range. The surface properties of a clean unfunctionalized gold surface were investigated. Using a computer-controlled acquisition system, a baseline was established for the resonant wavelength of an air-filled PDMS chamber. The real-time resonant wavelength shift is given in Fig. 3(a). After 35 min, methanol was injected into the chamber and data acquisition began once all the methanol had flowed over the gold surface and exited the 200 μm wide PDMS channel. Using the formulism provided in Ref. 19, which relates the adsorption thickness to the resonant wavelength shift, the dynamic adsorption thickness is plotted on the right side of Fig. 3(a). The adsorption thickness decreases from 10.7 to 6.3 nm over a 6.2 min span after the initial methanol rinse. Following water rinsing, however, the resonant wavelength shifts instantaneously with a relatively constant adsorption thickness of 0.2 nm over a 5.8 min span. The shift in the

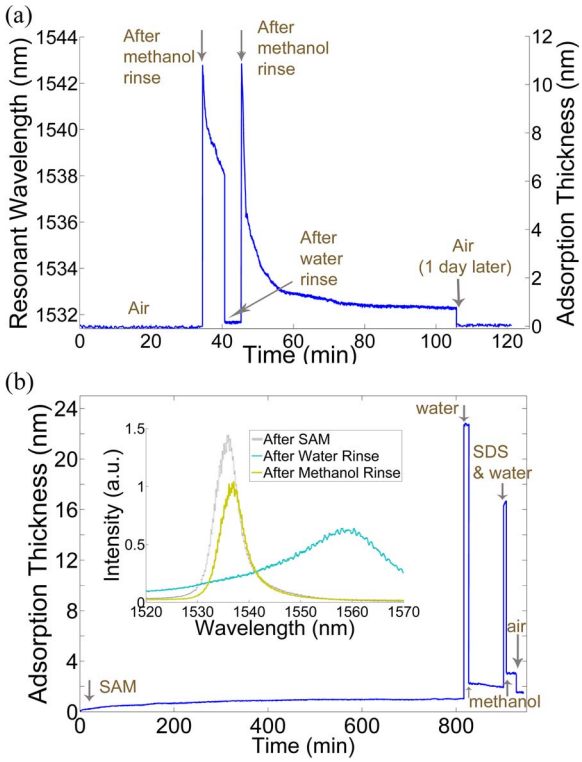

FIG. 3. (Color online) (a) Without SAM: the measured resonant wavelength shifts and the calculated adsorption thicknesses for the SPR sensor integrated with a PDMS channel for aqueous delivery of water and methanol. The surface is hydrophobic to water molecules but is wetted by methanol molecules. (b) With SAM: the calculated adsorption thickness shows that the SAM has modified the hydrophilicity property for water molecules from hydrophobic to hydrophilic while the surface now resists the wetting by methanol molecules. The insets show three spectra measured after SAM binding, water rinsing, and methanol rinsing.

resonant wavelength was monitored for a longer period after the second methanol rinse; an adsorbed methanol layer remains on the gold surface even after 60 min. This implies that a clean unfunctionalized gold surface can be wetted by methanol but is hydrophobic to water molecules. The adsorption thickness returns to baseline when measurement was performed a day later with air in the channel.

In order to modify the surface properties, 3-mercaptopropyl-trimethoxysilane was injected into the PDMS chamber and the chemical solution evaporated overnight. This produced a self-assembled monolayer (SAM) on the gold surface, as evident by the increasing absorption thickness as shown in Fig. 3(b). A similar procedure was conducted to determine the hydrophilicity of the Au-SAM surface to water and methanol molecules. The adsorption thickness after water rinsing was 22.7 nm, with no significant change over a 10-minute span. After methanol rinsing, however, the adsorption thickness decreases to only 2.0 nm. From Figs. 3(a) and 3(b), it can be seen that the adsorption thickness increases from 0.2 to 22.7 nm, which reveals that the SAM layer had modified the surface from hydrophobic to hydrophilic for water. The modified surface, however, resists the wetting by methanol where the adsorption thickness drops to 2.0 from 10.7 nm for the unmodified Au surface. In Fig. 3(b), the decaying behavior is not observed after water rinsing within the measurement time due to water's low vapor pressure in the chamber. Similar behavior occurs when the sensor was rinsed with a solution of 2% sodium dodecyl sulfate. The inset shows spectra after SAM formation, water rinsing, and methanol rinsing with the highest relative intensity of the former indicating the lowest adsorption thickness. This SPR method is being further investigated for quantitative hydrophilicity determination and comparison with the traditional contact angle approach.

In summary, a composite mushroomlike metallodielectric nanostructure was presented to enhance the normal electric field by coupling between localized plasmons and propagating SPPs. Although an enhancement factor of 1.4 is not extraordinary, the coupling approach shows promise. Optimized design employing LSPR coupling to propagating SPP modes and multiple SPP mode couplings are being studied. The fabrication method introduced here is a low cost and mass-producible technique to construct 3D composite nanostructures in which samples are reusable and reconfigurable. Tradeoffs between FWHM linewidth and deposition thickness, in terms of its effect on the transmission intensity, will create an optimized design in yielding the best resolution for the SPR sensor. Moreover, other SAM materials can also be used in order to engineer the material's surface properties for applications in biosensing, such as detection of protein interactions on the gold surface. Current ongoing investigations of antibody-antigen interactions using these SPR composite nanostructures are promising.

This work was partially funded by DARPA Center for Opto-Fluidic Integration and NSF. H.M. Chen acknowledges a fellowship and an ILIR funding from NAWCWD, China Lake.

[1] T. W. Ebbesen, H. J. Lezec, H. F. Ghaemi, T. Thio, and P. A. Wolff, Nature (London) **391**, 667 (1998).
[2] C. Nylander, B. Liedberg, and T. Lind, Sens. Actuators **3**, 79 (1983).
[3] D. C. Cullen, R. G. Brown, and C. R. Lowe, Biosensors **3**, 211 (1988).
[4] M. J. Jory, G. W. Bradberry, P. S. Cann, and J. R. Sambles, Meas. Sci. Technol. **6**, 1193 (1995).
[5] C. R. Lawrence, N. J. Geddes, D. N. Furlong, and J. R. Sambles, Biosens. Bioelectron. **11**, 389 (1996).
[6] A. G. Brolo, R. Gordon, B. Leathem, and K. L. Kavanagh, Langmuir **20**, 4813 (2004).
[7] K. A. Tetz, L. Pang, and Y. Fainman, Opt. Lett. **31**, 1528 (2006).
[8] M. E. Stewart, N. H. Mack, V. Malyarchuk, J. A. N. T. Soares, T.-W. Lee, S. K. Gray, R. G. Nuzzo, and J. A. Rogers, Proc. Natl. Acad. Sci. U.S.A. **103**, 17143 (2006).
[9] A. De Leebeeck, L. K. S. Kumar, V. de Lange, D. Sinton, R. Gordon, and A. G. Brolo, Anal. Chem. **79**, 4094 (2007).
[10] L. Pang, G. M. Hwang, B. Slutsky, and Y. Fainman, Appl. Phys. Lett. **91**, 123112 (2007).
[11] A. Lesuffleur, H. Im, N. C. Lindquist, and S.-H. Oh, Appl. Phys. Lett. **90**, 243110 (2007).
[12] P. R. H. Stark, A. E. Halleck, and D. N. Larson, Methods **37**, 37 (2005).
[13] W. Fan, S. Zhang, B. Minhas, K. Malloy, and S. R. J. Brueck, Phys. Rev. Lett. **94**, 033902 (2005).
[14] S. Wu, Q. Wang, X. Yin, J. Li, D. Zhu, S. Liu, and Y. Zhu, Appl. Phys. Lett. **93**, 101113 (2008).
[15] T. A. Kelf, Y. Sugawara, R. M. Cole, and J. J. Baumberg, Phys. Rev. B **74**, 245415 (2006).
[16] P. B. Johnson and R. W. Christy, Phys. Rev. B **6**, 4370 (1972).
[17] D. S. Kim, S. C. Hohng, V. Malyarchuk, Y. C. Yoon, Y. H. Ahn, K. J. Yee, J. W. Park, J. Kim, Q. H. Park, and C. Lienau, Phys. Rev. Lett. **91**, 143901 (2003).
[18] R. Muller, V. Malyarchuk, and C. Lienau, Phys. Rev. B **68**, 205415 (2003).
[19] L. S. Jung, C. T. Campbell, T. M. Chinowsky, M. N. Mar, and S. S. Yee, Langmuir **14**, 5636 (1998).